



**HAL**  
open science

## **Biaxial expansion due to compression experiments for measuring the failure strain of tubular samples**

Matthew Bono, Ahmed Zouari, T. Le Jolu, D. Le Boulch, H. Tabouret,  
Jérôme Crépin, Jacques Besson

► **To cite this version:**

Matthew Bono, Ahmed Zouari, T. Le Jolu, D. Le Boulch, H. Tabouret, et al.. Biaxial expansion due to compression experiments for measuring the failure strain of tubular samples. *Strain*, 2023, 10.1111/str.12462 . hal-04195533

**HAL Id: hal-04195533**

**<https://hal.science/hal-04195533>**

Submitted on 4 Sep 2023

**HAL** is a multi-disciplinary open access archive for the deposit and dissemination of scientific research documents, whether they are published or not. The documents may come from teaching and research institutions in France or abroad, or from public or private research centers.

L'archive ouverte pluridisciplinaire **HAL**, est destinée au dépôt et à la diffusion de documents scientifiques de niveau recherche, publiés ou non, émanant des établissements d'enseignement et de recherche français ou étrangers, des laboratoires publics ou privés.

# Biaxial expansion due to compression experiments for measuring the failure strain of tubular samples

M. Bono<sup>1</sup>  | A. Zouari<sup>1,2</sup> | T. Le Jolu<sup>1</sup> | D. Le Boulch<sup>1</sup> | H. Tabouret<sup>1</sup> | J. Crépin<sup>2</sup> | J. Besson<sup>2</sup>

<sup>1</sup>Université Paris-Saclay, CEA, Service d'Etude des Matériaux Irradiés, Gif-sur-Yvette, France

<sup>2</sup>MINES ParisTech, PSL Research University, MAT – Centre des Matériaux, CNRS UMR 7633, Evry, France

## Correspondence

Matthew Bono, Université Paris-Saclay, CEA, Service d'Etude des Matériaux Irradiés, 91191, Gif-sur-Yvette, France.  
Email: [matthew.bono@cea.fr](mailto:matthew.bono@cea.fr)

## Funding information

Project GAINES of the French Institut Tripartite CEA-EDF-Framatome

## Abstract

The failure strain of a tube is a function of the biaxial strain ratio (axial strain/hoop strain) to which it is subjected. The relationship between failure strain and the strain ratio can be determined experimentally using expansion due to compression tests with a tensile load (EDCT), in which a ductile pellet placed inside the tube is compressed axially so it expands in diameter and imposes a hoop strain on the tube. At the same time, a tensile load on the ends of the tube creates an axial strain. This study investigates the capabilities and limitations of EDCT tests using two devices that allow experiments to be performed on a standard tensile testing machine. The first device applies an axial force on the ends of the sample, and the second device applies an axial displacement. Tests on zirconium alloy tubes confirmed that the failure strain is dependent on the strain ratio and the metallurgical state of the material. EDCT tests can produce a range of strain ratios, but there is an upper limit on the strain ratio that can be obtained, and it is dependent on the plastic behaviour of the sample and the friction conditions between the components.

## KEYWORDS

biaxial testing, EDC, expansion due to compression, failure strain, nuclear fuel cladding

## 1 | INTRODUCTION

Many engineering applications require studies of the failure strain of thin-walled tubes subjected to biaxial loads in the hoop and axial directions, such as tube shaping and forming processes, hydroforming applications, tubes susceptible to fracture due to the freezing of internal fluids, strains imposed on nuclear fuel cladding and many others. The biaxial strain ratio on a tube (axial strain/hoop strain or  $\epsilon_{ZZ}/\epsilon_{\theta\theta}$ ) can have a significant effect on the hoop strain at which rupture occurs,<sup>[1]</sup> and many engineering problems require a precise understanding of this relationship. The effect of the strain ratio on the failure strain of sheet materials has been researched extensively,<sup>[2]</sup> but these results cannot necessarily be directly applied to tubular samples. Sheets and tubes often have very different mechanical properties due to the differences in their geometry and the respective processes used to fabricate them, which can affect the microstructure and the isotropy of the materials.<sup>[3]</sup> Therefore, it is often preferable to perform biaxial tests directly on tubular samples in order to measure the failure strain at different strain ratios. One means of performing this type of experiment is with

This is an open access article under the terms of the [Creative Commons Attribution](https://creativecommons.org/licenses/by/4.0/) License, which permits use, distribution and reproduction in any medium, provided the original work is properly cited.

© 2023 The Authors. *Strain* published by John Wiley & Sons Ltd.

an expansion due to compression test with a tensile load (EDCT), in which a tubular sample is loaded with a displacement-controlled hoop strain and a simultaneous axial load.<sup>[4,5]</sup> This type of experiment has historically required special testing machines with multiple actuators. The devices used in the current study were developed to allow EDCT tests to be performed on tubular samples using a standard tensile testing machine, thereby making this type of test much more accessible. This study investigates some of the advantages and limitations of EDCT tests, and it presents some results obtained using the devices.

This study was motivated by the need to experimentally measure the failure strain of fuel cladding tubes for nuclear reactors. In a pressurized water nuclear reactor, the fuel pellets are stacked inside cladding tubes that serve as the first of several barriers that contain the nuclear fission products, and their structural integrity is very important. The tubes are usually composed of a zirconium alloy, and each one has an outer diameter of 9.5 mm, a wall thickness of 0.6 mm and a length of approximately 4 m. The uranium oxide fuel pellets stacked inside the tubes have a height of 14 mm. The cladding tubes are arranged in assemblies that are submerged in the reactor core, where they heat water at a pressure of 155 bar to a temperature of 310°C. The pressurized hot water passes through a heat exchanger that produces steam that drives generators to produce electricity. Due to the presence of the hot fuel pellets, the temperature of the cladding tubes is generally around 350–400°C. The combination of the temperature and external pressure of the water causes each tube to decrease in diameter via creep, until its inner surface contacts the fuel pellets.

Any time the power of the reactor is adjusted, the temperature and diameter of the fuel pellets change. For example, whenever the reactor power is increased, the pellets expand in both diameter and height, as shown in Figure 1. When this occurs, the expansion of the pellet is imposed on the fuel cladding tube. Therefore, the cladding tube experiences an imposed hoop strain ( $\epsilon_{\theta\theta}$ ) and an axial strain ( $\epsilon_{zz}$ ). If these strains are severe enough, they could damage cladding tubes that have been embrittled by irradiation or the formation of hydrides. In order to guarantee the safe operation of the reactor, it is important to study the behaviour of the cladding tubes and the strain conditions in which they might rupture. The strain loading path, and in particular the strain biaxiality, can have a significant effect on the failure strain of the material<sup>[1,6]</sup> and is an important aspect of these studies. In the reactor, the strain ratio ( $\epsilon_{zz}/\epsilon_{\theta\theta}$ ) is known to fall between plane strain ( $\epsilon_{zz}/\epsilon_{\theta\theta} = 0$ ) and equi-axial conditions ( $\epsilon_{zz}/\epsilon_{\theta\theta} = 1$ ).<sup>[1]</sup> Thus, there is a need to develop laboratory experiments that can determine the failure strain of tubular samples in these biaxial loading conditions.

The two devices used in this study allow this type of experiment to be performed on tubular samples, with a strain biaxiality ratio ( $\epsilon_{zz}/\epsilon_{\theta\theta}$ ) in the range between 0 and 1, using a standard tensile testing machine. In both of these devices, the hoop strain is produced by compressing a ductile pellet inside the tubular sample so that it expands in diameter. In the first device, the axial strain is produced by applying an axial force to the ends of the sample via several plastically deforming tensile rods, and the strain ratio can be modified by changing the geometry of the rods.<sup>[7]</sup> The force required to achieve the desired strain ratio must be determined before the test so that appropriate tensile rods can be designed, and it is usually strongly dependent on the sample's mechanical behaviour. This device was introduced in a previous study,<sup>[8]</sup> in which it was used to develop a model for predicting the rupture of Zircaloy-4 cladding tubes via the accumulation of ductile damage. The second device applies an axial displacement (rather than a force) to the ends of the sample

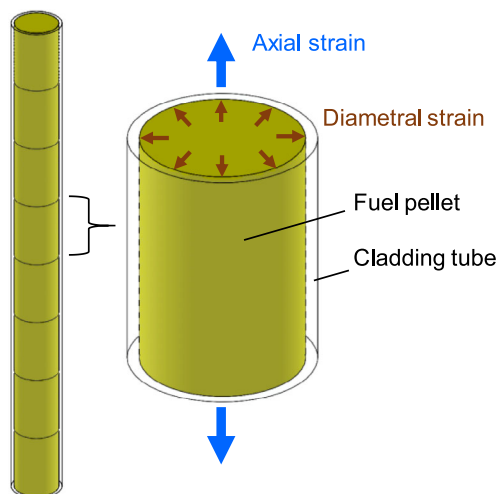


FIGURE 1 Axial and diametral strains of the fuel pellets stacked inside the cladding tube.

using a series of rigid linkages.<sup>[9]</sup> The strain ratio produced during the test is a function of the arrangement of the linkages, and it is relatively simple to perform an experiment with this device, as it does not require a precise knowledge of the sample's mechanical behaviour prior to the test.

In this study, experiments are performed using the two EDCT devices, and the relative advantages of applying either an axial force or an axial displacement to the ends of the sample are compared. Tests were performed using the two devices in order to demonstrate how the strain ratio and the metallurgical state of the material affect the failure strain. In addition, this study investigates the maximum value of the strain ratio that can be obtained using EDCT tests and the factors that affect this limit.

A summary of previous experimental methods that have been used to study the effect of the strain ratio on failure strain is presented in Section 2. Section 3 describes the experimental method, the operation of the devices, the effect of the coefficient of friction between the pellet and the tube and the method used to design the components. Section 4 presents the experimental results. Section 5 discusses how the strain biaxiality that can be produced in an EDCT test is limited and can be estimated by examining the yield locus of the sample material. The conclusions are presented in Section 6.

## 2 | PREVIOUS EXPERIMENTAL METHODS

Researchers have developed many different types of experiments in order to study the failure strain of materials as a function of the strain ratio. The most common method analyses the forming limit of sheet materials using drawing tests with a hemispherical punch and strip samples of varying width.<sup>[2]</sup> However, these tests cannot be used on tubular samples.

The most commonly used method of evaluating the failure strain of a tube is a burst test, in which an internal pressure is applied to a tube with closed ends.<sup>[10]</sup> Burst tests are commonly used to test materials for many different applications, and the equipment required for this type of test is readily available. In this test, a fluid, such as oil, is injected into the sample, which expands in diameter until it bursts. The external diameter of the tube is measured by a set of sensors, which usually measure the hoop strain at the mid-plane of the sample. An internal pressure test on a thin-walled tube produces a stress ratio ( $\sigma_{ZZ}/\sigma_{\theta\theta}$ ) of approximately 0.5, which leads to nearly plane strain conditions ( $\epsilon_{ZZ}/\epsilon_{\theta\theta} \approx 0$ ) for a material that respects the von Mises condition.<sup>[2]</sup> The test can also be modified by adding an axial force to the ends of the sample to vary the stress and strain ratios. One important characteristic of these types of tests is that the loads are an applied pressure and an applied force rather than applied displacements, so the sample experiences plastic instabilities prior to failure. A bulged region usually forms on the tube, and rupture occurs within this bulge.<sup>[11,12]</sup> The hoop strain sensors often measure the hoop strain at failure of the non-bulged portion of the tube,<sup>[13]</sup> but even if they measure the bulge, they are unable to measure the necking that can occur within the bulge prior to rupture.<sup>[12–15]</sup> Thus, the hoop strain at failure measured in this type of test is not fully representative of the applied displacement loading conditions experienced by fuel cladding.

A similar type of test is the modified burst test, in which a driver tube filled with hydraulic oil is inserted inside the tubular sample. A piston compresses the oil, and the resulting radial expansion of the driver tube is imposed on the sample. This type of test was designed to reproduce the load imposed on the fuel cladding by an expanding fuel pellet, and it has many advantages. For example, extremely high strain rates can be obtained to reproduce various strain-driven accident conditions.<sup>[16–19]</sup> Using a digital image correlation method and a series of mirrors, the strain fields can be measured over nearly the entire surface of the sample. Using this type of test, researchers have reported a variety of strain biaxiality ratios, including nearly plane strain conditions ( $\epsilon_{ZZ} \approx 0$ ) and positive strain ratios ( $\epsilon_{ZZ}/\epsilon_{\theta\theta} > 0$ ).<sup>[19]</sup> However, it is not clear to what extent the strain biaxiality ratio can be controlled during the test.

Another common test is a simple tension test. A tubular sample can be strained to failure in the axial direction, or a ring of material can be placed between two loading pins that pull it apart in the radial direction.<sup>[1]</sup> These tests can yield accurate measurements of the strain at failure for displacement-controlled loading, but only for pure axial or hoop loads.

The plane strain tensile test is a variation of the hoop tensile test and uses a wide, ring-shaped sample.<sup>[20]</sup> Two D-shaped dies pull the sample apart in the radial direction, and nearly plane strain conditions are obtained in the region between a set of notches on the ends of the sample. However, the strains produced in this type of test are concentrated into a zone of localized necking and are very heterogeneous. Therefore, it can be difficult to interpret the results.

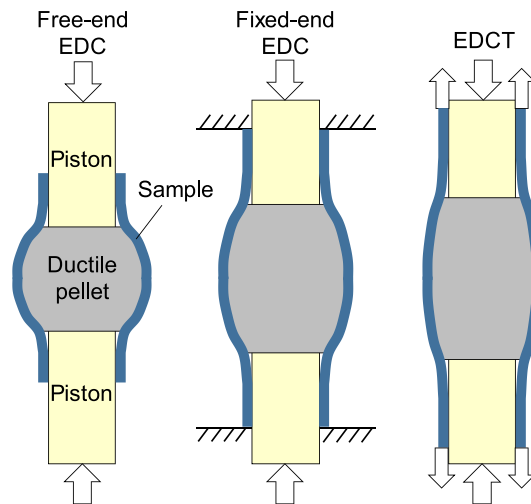


FIGURE 2 Free-end EDC test (left), fixed-end EDC test (centre) and EDCT test (right).

Displacement-controlled hoop strain loading of a tubular sample can be obtained with an expansion due to compression (EDC) test. In this test, a ductile cylindrical pellet is placed inside a tubular sample, where it is compressed axially, causing it to expand in diameter, thereby imposing a hoop strain on the tubular sample. Mishima<sup>[21]</sup> developed a test in which a ductile lead pellet was placed inside a beryllium tube. By compressing the lead pellet with two pistons so that it expanded in diameter, the failure hoop strain of the beryllium tube could be determined. Researchers have also placed a ductile pellet inside a ceramic expanding mandrel that imposes a hoop strain on the tube. This method has been used for stress corrosion cracking tests of tubes with an imposed hoop strain.<sup>[22]</sup> EDC tests can be used to study materials under extreme conditions, and they have been used in the nuclear industry to test the failure strain of irradiated fuel cladding tubes.<sup>[23–25]</sup>

In the original version of the EDC test, the ends of the tubular sample are free and unconstrained. During this type of free-end EDC test, the sample contracts axially as the central region expands in diameter, as shown in Figure 2. The strain biaxiality in the area of interest at the centre of the sample,  $\epsilon_{ZZ}/\epsilon_{\theta\theta}$ , is usually close to  $-0.5$ . In order to produce a greater strain ratio in the sample, the ends of the tubular sample have been restrained using various means to prevent it from contracting axially.<sup>[26,27]</sup> The end-restraining fixture used by Nobrega et al.<sup>[27]</sup> prevents any change in length of the sample, so the strain biaxiality is greater than that of a free-end test. Hellouin de Menibus et al.<sup>[28]</sup> used this type of fixed-end EDC test to study the effects of hydride blisters on the fracture of Zircaloy-4 tubes. They found that the hoop strain at failure for a fixed-end EDC test is significantly less than that of a free-end EDC test.

The strain biaxiality ratio produced in a fixed-end EDC test is generally close to  $-0.5$  at the beginning of the test, and it increases as the test progresses. Therefore, the strain biaxiality of a fixed-end EDC test is greater than that of a free-end EDC test, but it remains outside the range of interest of the current study ( $\epsilon_{ZZ}/\epsilon_{\theta\theta}$  between 0 and 1). However, biaxiality ratios that fall in this range can be obtained by applying a tensile load to the ends of the sample during an EDC test. For example, researchers have developed a type of EDC test in which the strain biaxiality can be controlled by applying an axial tensile load on the ends of the tubular sample as the ductile pellet is compressed inside of it.<sup>[4,5]</sup> Studies of pre-cracked specimens have shown that the hoop strain at failure tended to decrease as the strain biaxiality ( $\epsilon_{ZZ}/\epsilon_{\theta\theta}$ ) increased.<sup>[4]</sup> The device combines a tensile testing system and an EDC testing system, and it can produce displacement-controlled loading of a tubular sample with a large strain biaxiality ratio.

### 3 | EXPERIMENTAL METHOD

In the current study, two devices were used to perform EDCT tests, similar to those described above, but using a standard tensile testing machine. The devices do not require a special machine with two actuators (one actuator to compress the ductile pellet inside the sample and a second actuator moving in the opposite direction to apply the tensile load). Instead, each device can simultaneously compress the ductile pellet and apply an axial tensile load to the ends of

the tubular sample using a standard tensile testing machine with a single actuator.<sup>[7–9]</sup> Therefore, a special machine is not required, and EDCT tests can be performed in any laboratory equipped with a tensile testing machine.

### 3.1 | EDCT device with tensile rods

EDC tests are often performed on a tensile testing machine using a compression cage made of two rigid frames that slide relative to each other, as shown in Figure 3. Each frame consists of an outer plate and an inner plate, which are connected via two or more rigid bars. For example, *Outer plate 1* and *Inner plate 1* are connected via two rigid bars, as are *Outer plate 2* and *Inner plate 2*. The bars pass through the inner plates of the opposite frame. The two outer plates are connected to the load line of the tensile testing machine. When they are pulled apart, the two inner plates move towards each other, so a compression test can be performed between them.

In a free-end EDC test, pistons mounted to the two inner plates compress the ductile pellet inside the tubular sample. As the pellet plastically deforms, it expands in diameter, thereby imposing a hoop strain on the sample. In a fixed-end EDC test, an end-restraining fixture is added to prevent axial contraction of the sample. The samples are similar to those used by Hellouin de Menibus et al.<sup>[28]</sup> Each sample consists of a tube with a threaded cap welded to each end. Prior to welding the caps in place, a ductile pellet and two stainless steel discs are inserted inside the sample. The ends of the sample are passed through the rigid frame of the restraining fixture, and a nut is screwed onto each threaded cap so that the fixture will prevent any axial contraction of the tube during the test. Each threaded cap contains a central hole so that a piston can pass through it in order to compress the pellet. The strain biaxiality achieved with this type of fixed-end EDC test is generally close to  $-0.5$  at the beginning of the test and increases as the test progresses.

Greater values of strain biaxiality can be achieved by replacing the end-restraining fixture with a guide consisting of two plates mounted to columns that can elongate telescopically to allow an axial tensile load to be applied to the sample. As shown in Figure 4, the nuts screwed onto the ends of the sample are seated against the outer surfaces of the plates. The guide is manipulated by tensile rods and assures that the force exerted on the sample is purely axial.<sup>[8]</sup>

In this study, there are four tensile rods, two of which are attached to each half of the guide. The opposite end of each rod is attached to one of the outer plates of the compression cage. Each tensile rod passes through a hole in the opposite inner plate. During an EDCT test, the outer plates of the cage are pulled apart by the tensile testing machine. The blue components in Figure 4 move downwards, and the yellow components move upwards. The outer plates apply a tensile force to the ends of the tubular sample via the tensile rods and the axial guide. The inner plates move towards each other and compress the pellet inside the sample via the pistons, as in the free-end and fixed-end EDC tests.

One very important aspect of the device is that the tensile rods are designed to deform plastically during the test, and the axial force that they apply to the sample is a function of their geometry, yield strength and strain hardening

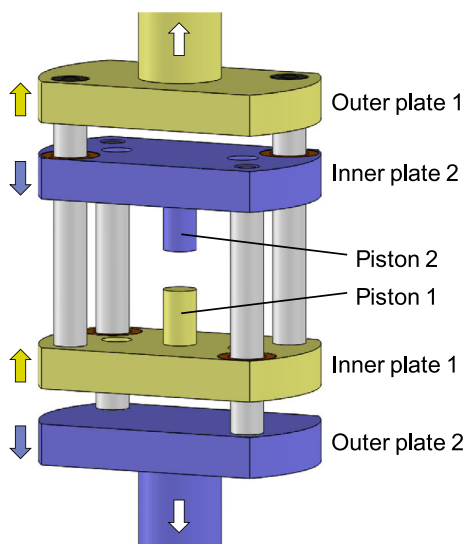


FIGURE 3 Compression cage for EDC tests.

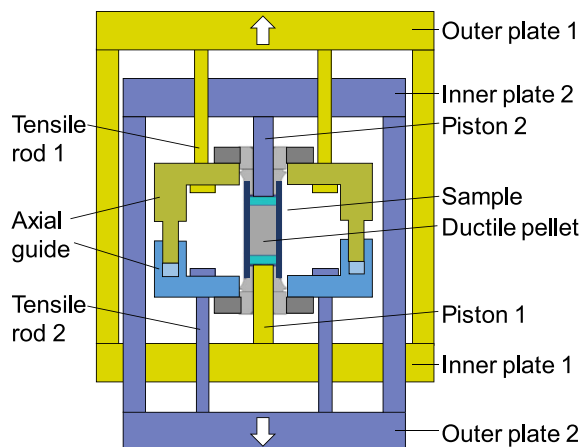


FIGURE 4 EDCT device with tensile rods.<sup>[7]</sup>

characteristics. The material and geometry of the tensile rods must be selected carefully in order to obtain a tensile force that leads to the desired strain biaxiality.

If the experimenter wishes to apply a nearly constant axial force to the sample, the material selected for the tensile rods should have a relatively flat engineering stress–strain curve, such as cold-worked steel. In this case, the force in each rod will be equal to the yield strength multiplied by the cross-sectional area. However, in most cases, in order to obtain the desired strain biaxiality ratio in the centre of the sample, the tensile force must increase as the test progresses. In this case, the tensile rods should be made of a material that strain hardens appropriately. The initial force in the rods will be equal to the yield strength multiplied by the cross-sectional area, and the force will increase thereafter and follow the engineering stress–strain curve of the material. Therefore, the strain hardening rate of the rods is very important. In addition, the length of the gauge section of the tensile rods will affect the load–displacement curve. Shorter rods will experience greater strain for a given displacement, and thus, the axial load will increase more quickly. In contrast, longer rods will lead to a smaller rate of increase of the axial force. The rods should also be designed so that they do not deform beyond their necking strain.

The key aspect in implementing the device lies in the design of the tensile rods, which must be selected in order to achieve the desired hoop and axial strains in the central region of the sample. The plastically deformed tensile rods must be replaced after each test.

### 3.1.1 | Design of the tensile rods

The tensile rods were designed with the aid of finite element simulations using the CAST3M finite element code.<sup>[29]</sup> The simulations are almost identical to those described in a previous study.<sup>[8]</sup> The two-dimensional (2D) axisymmetric finite element model is shown in Figure 5. The model uses quadrangular quadratic finite elements with eight nodes and four G points and consists of four components: the tubular sample, the ductile pellet, the rigid piston and the tensile rod.

The left side of Figure 5 is the rotational axis of symmetry, where the nodes are constrained in the radial ( $r$ ) direction. The bottom edge of the figure is a plane of symmetry, where the nodes are constrained in the axial ( $z$ ) direction.

In the experiments, the axial guide transmits the force of the tensile rods to the ends of the sample. To simplify the simulations, the axial guide is not included in the simulation, and the two tensile rods are modelled as a single component of appropriate cross section on the axis of the tube. A constraint is imposed such that the bottom surface of the tensile rod experiences the same displacement as the top surface of the sample. In Figure 5, the tensile rod is shown as being directly attached to the sample, which is visually representative of the experimental set-up.

The motion of the plates of the compression cage is modelled by imposing axial (vertical) displacements on the upper surfaces of the piston and the tensile rod, as indicated by the arrows in Figure 5. The upper surface of the piston is displaced downwards at a rate of 0.002 mm/s, and the upper surface of the tensile rod is displaced upwards at this

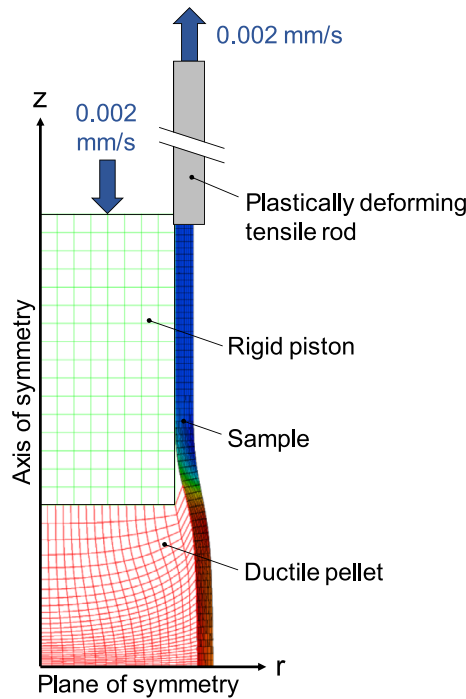


FIGURE 5 Finite element model of the EDCT test.

same rate. Thus, the piston compresses the pellet, causing it to expand in diameter and push the central portion of the tubular sample outwards in the radial direction. At the same time, the tensile rod is stretched in tension so that it exerts an axial tensile force on the end of the sample.

The time-dependent, non-linear, plastic deformation of the components is calculated by discretizing the problem into several hundred time steps with the CAST3M software. Because the model experiences large plastic deformations with significant nodal displacements, the geometry of the model must be updated at each time step.

### 3.1.2 | Material models

The mechanical behaviour of the polytetrafluoroethylene (PTFE) pellet was calculated from data from compression tests.<sup>[28]</sup> An elastic isotropic model was used for the elastic phase, and a plastic isotropic model with linear isotropic strain hardening was used for the plastic phase. The flow stress of the polymer pellet is given by Equation (1).

$$\bar{\sigma} = \sigma_y + K \bar{\epsilon}_p^n \quad (1)$$

$\bar{\epsilon}_p$  is the equivalent plastic strain.  $\sigma_y$  is the yield strength and is equal to 8 MPa.  $K$  is a strength coefficient and is equal to 30 MPa.  $n$  is a strain hardening exponent and is equal to 0.5. Young's modulus is assumed to be 0.6 GPa, and Poisson's ratio is assumed to be 0.47.

The cold-worked stress-relieved (CWSR) Zircaloy-4 cladding tube was modelled using a simplified version of the anisotropic behaviour law developed by Le Saux et al.<sup>[30]</sup> The plastic orthotropy of the material is described using Hill's anisotropic yield criterion<sup>[31]</sup> with isotropic hardening, in a cylindrical coordinate system. The equivalent stress  $\sigma_H$  is given by Equation (2), where  $H_{rr} = 0.58$ ,  $H_{\theta\theta} = 0.42$ ,  $H_{zz} = 0.41$  and  $H_{r\theta} = H_{rz} = H_{\theta z} = 1.5$ .

$$\sigma_H = [H_{rr}(\sigma_{\theta\theta} - \sigma_{zz})^2 + H_{\theta\theta}(\sigma_{zz} - \sigma_{rr})^2 + H_{zz}(\sigma_{rr} - \sigma_{\theta\theta})^2 + 2H_{r\theta} \cdot \sigma_{r\theta}^2 + 2H_{rz} \cdot \sigma_{rz}^2 + 2H_{\theta z} \cdot \sigma_{\theta z}^2]^{1/2} \quad (2)$$

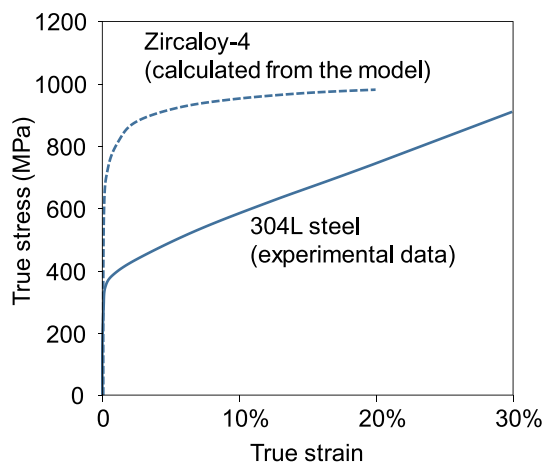


FIGURE 6 Stress-strain curves for Zircaloy-4 and 304L steel.

The yield surface is expressed as  $\sigma_H - R(p) = 0$ , where  $R(p)$  represents isotropic hardening and  $p$  represents the cumulated plastic strain associated with the Hill model. This function is plotted in Figure 6. The plastic strain rate tensor is then calculated from the normality rule. Young's modulus is assumed to be 95 GPa, and Poisson's ratio is assumed to be 0.34. Complete details of the model are given in Le Saux et al.<sup>[30]</sup>

The tensile rods used in this study were composed of 304L austenitic stainless steel, which was selected because it has the necessary work hardening rate to increase the axial force on the sample throughout the test to achieve the desired strain ratio. The measured true stress-strain curve from a tensile test<sup>[8]</sup> is shown in Figure 6 and was used directly in CAST3M, assuming von Mises plasticity. The piston was modelled as a rigid solid.

### 3.1.3 | Friction conditions

The frictional interactions between the components are very complex, and the boundary conditions at the interfaces in the simulations must be chosen carefully. The contact surfaces are modelled using Coulomb's law of friction, which is implemented in the CAST3M software. A series of simulations revealed that the value of the coefficient of friction between the piston and the pellet has a negligible effect on the computed sample behaviour. Therefore, this interface is modelled as frictionless in order to reduce the computation time.

In contrast, the coefficient of friction between the pellet and the tubular sample has a significant effect on the calculated strain biaxiality at the centre of the sample. Therefore, careful attention must be given to this parameter. Several measured values for static and dynamic coefficients of friction between PTFE and various metals have been reported in the literature. Values ranging from 0 to 0.4 have been reported by previous researchers for the coefficient of friction between PTFE and steel.<sup>[32-34]</sup> It appears that the experimental method and the test conditions can have a significant effect on the measured coefficient of friction. Values of the coefficient of friction used by researchers in simulations of free-end EDC tests on zirconium alloy samples include 0 (frictionless) for a polymer pellet,<sup>[35]</sup> 0.1 for a PTFE pellet<sup>[36,37]</sup> and 0.4 for a polymer pellet.<sup>[1]</sup>

In order to select a value of the coefficient of friction between the PTFE pellet and the Zircaloy-4 sample, simulations of a fixed-end EDC test were performed using values of 0.1, 0.2 and 0.4. The hoop and axial strains measured at the centre of the sample for two fixed-end EDC tests are compared to the simulations in Figure 7. The strains were measured using a stereo digital image correlation system, as described in Section 3.3. The closest agreement with the experimental data is found for the simulation with a coefficient of friction of 0.4.

### 3.1.4 | Selected tensile rod geometry

Several simulations were performed in order to estimate appropriate values for the length and diameter of the tensile rods using a coefficient of friction of 0.4 between the pellet and the sample. The simulations indicate that a strain

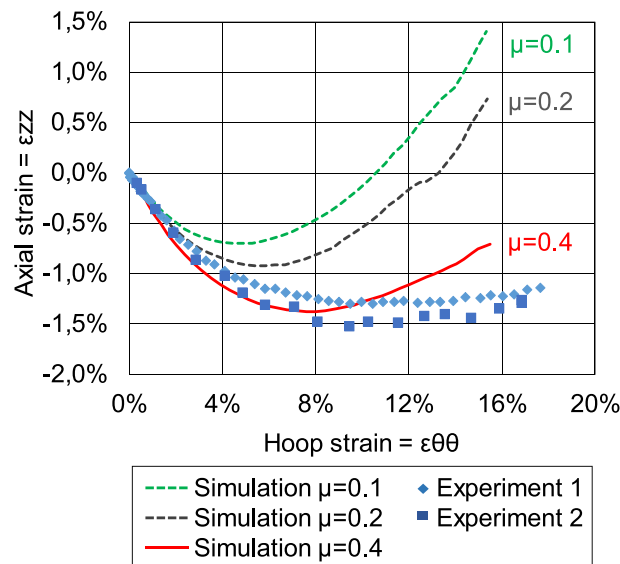


FIGURE 7 Measured and simulated strains for fixed-end EDC tests.

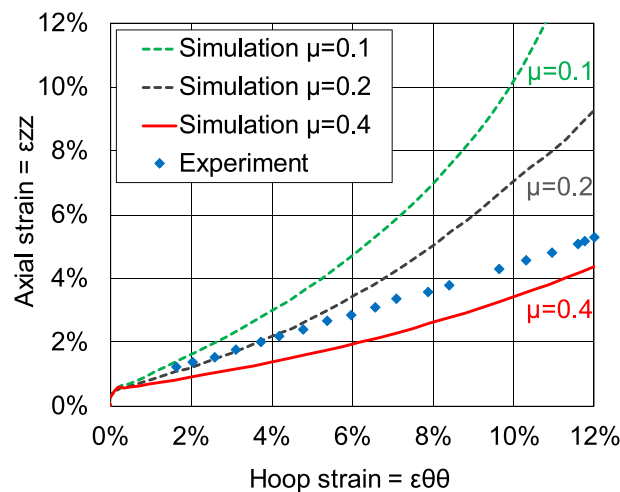


FIGURE 8 Measured and simulated strains for an EDCT test.

biaxiality ratio,  $\varepsilon_{zz}/\varepsilon_{\theta\theta}$ , of approximately 0.4 could be obtained with tensile rods of length 60 mm and cross section 20 mm<sup>2</sup>, as shown by the solid red curve in Figure 8.

Simulations using this same tensile rod design and coefficients of friction of 0.1 and 0.2 are also shown by the dashed curves in Figure 8. The coefficient of friction has a significant effect on the axial strain, because a greater coefficient of friction leads to a larger frictional force that opposes the axial force applied by the tensile rods. Thus, a greater coefficient of friction leads to a smaller axial strain and a smaller strain ratio, as seen in the figure.

### 3.2 | EDCT device with a controlled axial displacement

The second EDCT device was developed in this study and applies a controlled axial displacement to the ends of the sample during the test.<sup>[9]</sup> Therefore, it is not necessary to calculate the axial force required on the sample, and the simulations described above are not necessary. Furthermore, there are no tensile rods or other components that need to be replaced after each test.

This device also uses a compression cage made of two rigid frames that slide relative to each other, and the pistons that compress the ductile pellet inside the tubular sample are mounted on the plates. For this device, the axial guide

has been replaced with a mechanism that is driven by a series of linkages attached to the compression cage, as shown in Figure 9. The linkages move an additional pair of plates in the axial direction to impose an axial displacement on the ends of the sample. By altering the relative lengths of the lever arms, the ratio of the displacement of the ends of the sample to the displacement of the pistons can be modified. For example, to reduce the displacement ratio, point A can be moved further from point B. To increase the displacement ratio, point A can be moved closer to point B.

As discussed in Section 4.2, for many materials, a given displacement ratio produces a similar strain ratio ( $\epsilon_{ZZ}/\epsilon_{\theta\theta}$ ) in the centre of the sample. Thus, the same device can be used to compare different materials, provided their mechanical behaviours are not vastly different.

### 3.3 | Strain measurements

Before each test, the tubular sample is painted with a white background, and then a random speckle pattern is applied using black spray paint, which allows the strain field to be measured using digital image correlation. The speckle pattern can be seen in Figure 10, which depicts typical ruptured samples with an axial crack (left) and a circumferential crack outside the area of interest (right).

For the EDCT tests performed using the device with tensile rods, the hoop and axial strains in the central portion of the tubular sample were measured using a stereo digital image correlation system and the VIC-3D commercial software.

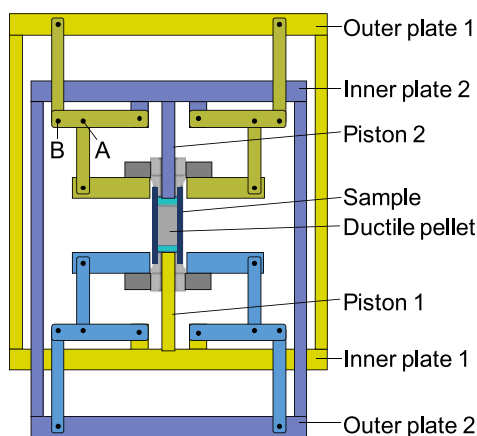


FIGURE 9 EDCT device with a controlled axial displacement.<sup>[9]</sup>

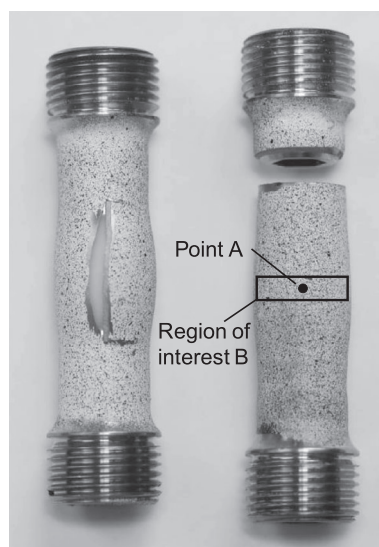


FIGURE 10 Ruptured samples with an axial crack (left) and a circumferential crack (right).

This system was also used for the free-end and fixed-end EDC tests. The parameters for the digital image correlation are indicated in Table 1. The system uses two cameras with a resolution of  $2048 \times 2048$  pixels, a focal length of 50 mm and an aperture of  $f/22$ . The stand-off distance is approximately 800 mm, and the stereo angle is approximately  $20^\circ$ . The image scale is  $34.5 \mu\text{m}/\text{pixel}$ . The acquisition rate is two images per second. The correlation analyses in the software use a subset size of 27 pixels with a step size of 7 pixels. The calculated Green–Lagrange strain fields are treated with a Gaussian spatial filter before analysing the results. The Green–Lagrange strains calculated by the software are converted to logarithmic true strains. The system can measure the three-dimensional displacements and strains over the front face of the sample, in the area that is simultaneously visible to both cameras. The strains correspond to a point at the centre of the face of the sample, where the hoop strain is greatest. An example of this point is labelled ‘A’ in Figure 10.

To evaluate the noise floor, the displacement fields and strain fields of the sample were calculated between static images, and the standard deviations are reported in Table 1. The accuracy of the calculated strains was estimated by comparing a measurement made by digital image correlation with a laser-scan micrometer measurement, for a sample that was subjected to an interrupted free-end EDC test. The test was stopped at a hoop strain of 34%, and the sample did not rupture. The absolute difference between the hoop strains measured using the two methods was approximately 0.3%.

The stereo digital image correlation system was not available for the EDCT tests using the device with a controlled axial displacement, so the strains were measured using a 2D digital image correlation system with a single camera with resolution  $2448 \times 2048$  pixels. The parameters are indicated in Table 2. The lens has a focal length of 35 mm and an aperture of  $f/16$ , and the stand-off distance is 220 mm. The image scale is  $20.8 \mu\text{m}/\text{pixel}$ . The image correlation for these tests is performed using GOM Correlate with a subset size of 20 pixels and a step size of 10 pixels. The hoop and axial

**TABLE 1** Stereo digital image correlation parameters.

Camera	Allied Vision Manta R G-419B
Image resolution	2048 pixels $\times$ 2048 pixels
Region of interest	500 pixels $\times$ 900 pixels
Lens	Schneider Xenoplan 2.8/50
Lens focal length	50 mm
Aperture	$f/22$
Field of view	Approximately $71 \times 71$ mm
Image scale	$34.5 \mu\text{m}/\text{pixel}$
Stereo angle	$20^\circ$
Stand-off distance	800 mm
Image acquisition rate	2 Hz
Patterning technique	Base coat of white spray paint with sprayed black paint speckles
Pattern feature size (approximate)	0.1–0.2 mm
DIC software	Correlated Solutions, VIC-3D version 8.4.0
Image filtering	Gaussian spatial filter with a kernel size of 15
Subset size	27 pixels = 0.93 mm
Step size	7 pixels = 0.24 mm
Subset shape function	Affine
Matching criterion	Zero-normalized squared differences
Interpolant	8-tap spline
Strain window	5, 7 or 9
Virtual strain gauge size	55–83 pixels = 1.9–2.9 mm
Strain formulation	Green–Lagrange, converted to true strain
Post-filtering of strains	No temporal filter was used
Strain noise floor	$<600 \mu\text{m}/\text{m}$

TABLE 2 2D digital image correlation parameters.

Camera	Baumer VCXG-51M.I
Image resolution	2448 pixels × 2048 pixels
Region of interest	Approximately 460 pixels × 120 pixels
Lens	KOWA 35 mm
Lens focal length	35 mm
Aperture	f/16
Field of view	Approximately 51 × 43 mm
Image scale	20.8 μm/pixel
Stereo angle	N/A
Stand-off distance	220 mm
Image acquisition rate	1 Hz
Patterning technique	Base coat of white spray paint with sprayed black paint speckles
Pattern feature size (approximate)	0.1–0.2 mm
DIC software	GOM Correlate 2019
Image filtering	Images are not filtered prior to the analysis
Subset size	20 pixels = 0.42 mm
Step size	10 pixels = 0.21 mm
Subset shape function	Affine
Matching criterion	Sum square difference normalized to zero
Interpolant	Bilinear
Strain window	Strain tensor neighbourhood = 1
Virtual strain gauge size	An average filter is applied over the entire region of interest
Strain formulation	Engineering strain, converted to true strain
Post-filtering of strains	No temporal filter was used
Strain noise floor	<70 μm/m after filtering over the region of interest

strains are calculated by creating a region of interest over the width of the sample with a height of 2.4 mm. This region is located at the axial position of the maximum hoop strain. An example of this region is labelled 'B' in Figure 10. The average hoop strain and average axial strain are calculated over this region for each image, and the engineering strain calculated by the software is converted to logarithmic true strain. To estimate the accuracy of the strain measurements, an interrupted free-end EDC test was also performed with this system. The test was stopped at a hoop strain of 28%, and the absolute difference between the hoop strains measured using this system and a laser was approximately 0.3%.

## 4 | EXPERIMENTAL RESULTS

### 4.1 | EDCT tests on CWSR Zircaloy-4

EDCT tests were performed on tubular fuel cladding samples composed of CWSR Zircaloy-4 at room temperature. The tubes had an outer diameter of 9.5 mm and wall thickness of 0.6 mm. The length of each sample was 27 mm. The ductile pellet inside the sample was composed of PTFE with a diameter of 8.3 mm and height 14 mm.

Initially, free-end and fixed-end EDC tests were performed. In the free-end EDC test, the strain biaxiality ratio was approximately  $-0.5$  at the beginning of the test and increased thereafter. The sample reached a strain biaxiality ratio of  $-0.3$  and a hoop strain of 44% when the test was stopped, but it did not rupture. Two fixed-end EDC tests were performed. For these tests, the strain ratio was initially  $-0.4$  and increased to  $-0.1$  when the samples fractured at hoop strains of 18% and 17%. Each crack initiated at the centre of the sample, where the hoop strain was greatest, and it was

oriented parallel to the tube axis. This type of rupture is similar to that shown on the left side of Figure 10 and is consistent with a primary strain in the hoop direction.

Several EDCT tests were then performed using the device with tensile rods. The first test used tensile rods of length 60 mm and cross section 20 mm<sup>2</sup>. The sample ruptured at a hoop strain of 12% and an axial strain of 5.3%. Thus, the strain biaxiality ratio,  $\epsilon_{zz}/\epsilon_{\theta\theta}$ , was 0.44 when the sample ruptured. The measured strains are represented by the curve the furthest to the right in Figure 11, and the values represent the measurements at the centre of the sample.

Several additional tests were performed using tensile rods of different diameters, and the strain paths are plotted in Figure 11. The strain biaxiality ratios for these tests ranged from 0.20 to 0.44, and the hoop strains at failure were approximately 12%.

EDCT tests were also performed using the device that applies a controlled axial displacement to the ends of the sample. For these tests, the linkages were arranged such that the axial displacement of each end of the sample was approximately one-tenth the displacement of each piston. Two EDCT tests were performed on CWSR Zircaloy-4 samples using this configuration, and the measured strains are plotted in Figure 11. For these tests, the values in the graph represent the average in the region of interest of height 2.4 mm. The samples ruptured at hoop strains of 11% and 12%, and strain ratios of 0.09 and 0.10.

These tests confirmed the effect of the strain ratio on the hoop strain at rupture, as well as the capacity of the EDC tests to produce a wide range of strain biaxiality ratios using a standard tensile testing machine. The data for CWSR Zircaloy-4 shown in Figure 11 indicate that the rupture strain decreases as the strain ratio increases up to 0, and it is relatively constant for strain ratios between 0 and 0.44. This same trend was observed in a previous study,<sup>[8]</sup> in which EDCT tests with tensile rods were performed on the same sample material. However, in the previous study, the wall thickness of each tubular sample had been reduced by 9% over the central portion of its length in order to force rupture to occur in the centre, and the objective of that study was to investigate the failure of the tubes via the accumulation of ductile damage. In the current study, the objective is to investigate the range of strain ratios that can be produced with EDCT tests without altering the wall thickness. It was discovered that a strain ratio greater than 0.44 could not be produced for this material in these conditions. Attempts to obtain a greater strain ratio resulted in rupture outside the area of interest of the sample, and the reason for this phenomenon is discussed in Section 5.

## 4.2 | EDCT tests on cold-worked and heat-treated Zircaloy-4

EDCT tests were performed on several materials with different mechanical properties. In order to use the device with tensile rods, it would be necessary to perform simulations for each material to identify an appropriate material and geometry for the tensile rods. Therefore, the device that applies a controlled axial displacement to the ends of the sample was used for these tests, because it does not require this type of calculation. The linkages were arranged such that the axial displacement of each end of the sample was approximately one-tenth the displacement of each piston. In addition to the two EDCT tests on CWSR Zircaloy-4 described above, additional tests were performed on cold-worked

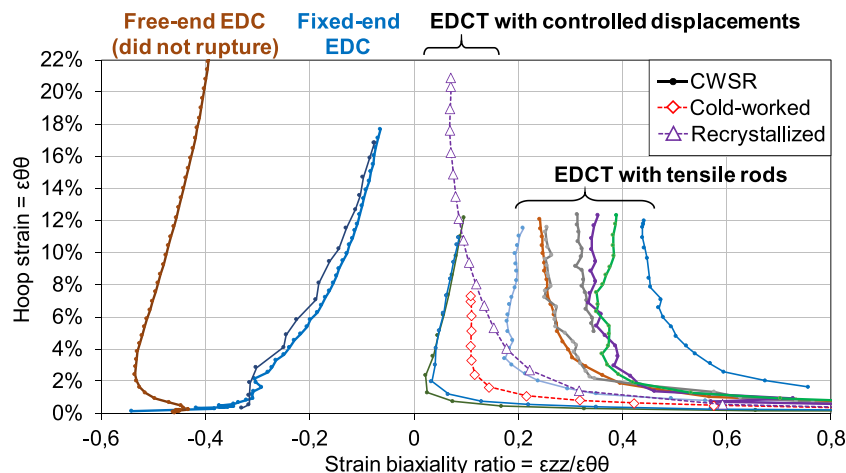


FIGURE 11 Measured strains for different EDC tests on Zircaloy-4 tubes.

Zircaloy-4 and recrystallized Zircaloy-4. The objective of these tests was to demonstrate the ability of the EDCT device to reproduce the same strain ratio on different materials, as well as to demonstrate the effect of the metallurgical state of the material on the failure strain. These tests are shown by the dashed curves in Figure 11. Despite the different mechanical properties of the cold-worked, CWSR and recrystallized samples, the final strain ratios were very similar (0.11 for the cold-worked sample, 0.09 and 0.10 for the CWSR samples and 0.07 for the recrystallized sample). However, the hoop strains at failure were significantly different (7% for the cold-worked sample, 11% and 12% for the CWSR samples and 21% for the recrystallized sample). The cold-worked sample exhibited the smallest failure strain, and the recrystallized sample exhibited the largest failure strain. Thus, EDCT tests with controlled axial displacements are a good means of producing similar strain ratios for samples with different mechanical properties in order to compare their failure strains.

## 5 | DISCUSSION

EDCT tests can produce a wide range of strain ratios, but there is an upper limit on the strain ratio that can be obtained in the sample during the test. As discussed below, this limit is affected by the friction conditions between the pellet and the sample, and the shape of the yield locus of the sample material can also affect this limit.

### 5.1 | Limit on the strain biaxiality ratio

For the CWSR Zircaloy-4 tubes and test conditions used in this study, attempts to obtain a strain biaxiality ratio greater than 0.44 resulted in rupture outside the area of interest. Due to the excessive axial tensile force, the sample ruptured in tension near the welded cap, as shown on the right side of Figure 10. The reason for this rupture is related to the load biaxiality ratios in the different zones of the sample. The centre of the sample experiences biaxial loading in the hoop and axial directions. However, the ends of the sample are loaded in pure tension, so the stress is predominantly tensile in the space between the welded caps and the pellet. If the axial stress exceeds the ultimate tensile strength of the material, localized necking and failure in tension will occur in this region. In this case, the test does not provide the desired information about the failure strain in the area of interest. This limit on the axial stress affects the achievable strain biaxiality in the centre of the sample. The achievable strain biaxiality can be examined, in simplified phenomenological terms, by examining the yield locus of a theoretical sample material. To simplify the discussion, the material is assumed to have perfectly plastic behaviour with negligible strain hardening.

Many engineering materials exhibit plastic anisotropy due to the texture created during sheet or tube manufacturing processes. For example, materials such as titanium and zirconium alloys tend to have a greater yield strength in equi-biaxial loading than in simple tension. In contrast, certain aluminium and magnesium alloys can be weaker in equi-biaxial loading.<sup>[38–40]</sup> The CWSR Zircaloy-4 tubes used in the current study have a particular texture due to the hexagonal close-packed crystal structure and the orientation of the grains resulting from the tube manufacturing process.<sup>[3]</sup> Figure 12 presents an example of a yield locus, based on Hill's anisotropic plasticity theory<sup>[31]</sup> with parameters  $H_{rr} = 0.58$ ,  $H_{\theta\theta} = 0.42$  and  $H_{zz} = 0.41$ . These values correspond to CWSR Zircaloy-4 at 25°C.<sup>[30]</sup> In the sample, the

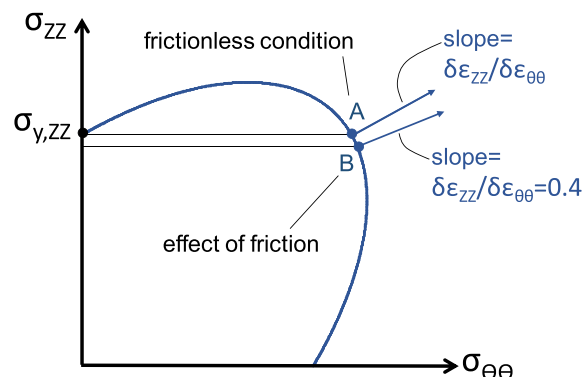


FIGURE 12 Hill's anisotropic yield locus. The limiting strain biaxiality ratio is given by the slope of the normal to the yield locus ( $\delta\epsilon_{zz}/\delta\epsilon_{\theta\theta}$ ).

radial stress,  $\sigma_{rr}$ , and the shear stresses are small compared to the axial and hoop stresses and can be neglected, so Hill's equivalent stress can be written in the form of Equation (3).

$$\sigma_H^2 = H_{rr}(\sigma_{\theta\theta} - \sigma_{zz})^2 + H_{\theta\theta}(\sigma_{zz})^2 + H_{zz}(\sigma_{\theta\theta})^2 \quad (3)$$

If the material is loaded in pure axial tension, then it will yield when the stress reaches the axial yield strength,  $\sigma_{y,ZZ}$ , as indicated in Figure 12. It is important to note that the yield strength of this material is greater in equi-biaxial tension than in pure axial tension.

In the simple, theoretical case of a frictionless interface between the pellet and the sample, the axial stress in the centre of the sample would be approximately equal to the axial stress at the ends of the sample. For the limiting case, this condition is represented by point 'A' in Figure 12. According to the principle of normality,<sup>[2,41]</sup> a plastic strain increment vector is normal to the yield surface. For a frictionless pellet-sample interface and a biaxial loading path that intersects the yield locus at an axial stress of  $\sigma_{y,ZZ}$ , the normal to the yield locus has a slope of  $\delta\varepsilon_{ZZ}/\delta\varepsilon_{\theta\theta}$ , which is the limiting value of the strain biaxiality for an EDCT test. Achieving a larger strain biaxiality would require a larger axial stress, which is not possible for a perfectly plastic material because the sample would fail in tension between the welded caps and the pellet, as was the case for the sample shown on the right side of Figure 10. Differentiating Equation (3) yields Equation (4). This equation can be used to estimate the limiting value of the strain biaxiality, which corresponds to the point where  $\sigma_{ZZ} = \sigma_{y,ZZ}$ .

$$\frac{\delta\varepsilon_{ZZ}}{\delta\varepsilon_{\theta\theta}} = \frac{\sigma_{ZZ}(H_{rr} + H_{\theta\theta}) - H_{rr}\sigma_{\theta\theta}}{\sigma_{\theta\theta}(H_{rr} + H_{zz}) - H_{rr}\sigma_{zz}} \quad (4)$$

In reality, the friction between the pellet and the sample reduces the achievable strain biaxiality ratio. In the experiment, the ductile pellet is compressed in the axial direction as the sample is extended in the axial direction, and there is a significant contact pressure between them. Thus, the ductile pellet exerts an axial frictional force on the sample, so the axial stress at the centre of the sample is reduced, as represented by point 'B' in Figure 12. The normal to the yield locus at point 'B' has a smaller slope than the normal at point 'A'. In other words, the achievable strain biaxiality,  $\delta\varepsilon_{ZZ}/\delta\varepsilon_{\theta\theta}$ , is reduced by the friction between the sample and the pellet. The normal to the yield locus at point 'B' in Figure 12 is drawn with a slope of 0.4, in order to correspond to the experimentally determined limiting value.

## 5.2 | Effect of the yield locus

The shape of the yield locus has a significant effect on the limiting value of the strain biaxiality ratio that can be achieved in an EDCT test. For example, in the case of the von Mises yield locus with an equi-biaxial load and a frictionless pellet-sample interface, at the limiting tensile stress value ( $\sigma_{y,ZZ}$ ), the normal to the yield locus has a slope of  $\delta\varepsilon_{ZZ}/\delta\varepsilon_{\theta\theta} = 1$ , as shown by the dashed curve in Figure 13. Thus, the theory predicts that the EDCT method should be able to produce strain biaxiality ratios of up to 1 for a material with this type of yield locus. If friction is considered at the pellet-sample interface, then the normal to the yield locus has a smaller slope, and the achievable strain biaxiality ratio is reduced, as shown in the figure.

Even greater strain ratios should be possible with other sample materials. Many common engineering materials, such as certain aluminium and magnesium alloys, can have a smaller yield strength in equi-biaxial loading than in simple tension.<sup>[38-40]</sup> An example of a yield locus for such a material is shown by the dotted curve in Figure 13. At the limiting tensile stress value ( $\sigma_{y,ZZ}$ ), the normal to the yield locus has a greater slope compared to the other cases presented in the figure. Thus, the EDCT test is predicted to be able to achieve an even larger strain ratio for this material than for the other materials shown in the figure.

The discussion above considers the case of Hill's anisotropic yield locus, of which the von Mises locus is a special case. There are many other forms of yield loci, both theoretical and experimental.<sup>[2]</sup> Regardless of its form, the yield locus can be used along with the principle of normality to estimate the theoretical limiting strain ratio that can be achieved in an EDCT test for a perfectly plastic material by determining the slope of the normal to the yield locus,  $\delta\varepsilon_{ZZ}/\delta\varepsilon_{\theta\theta}$ , at the axial tensile yield strength of the material. This method provides only an estimate, because the friction

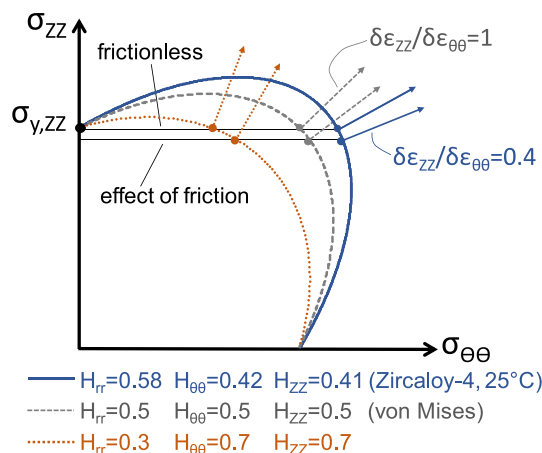


**FIGURE 13** Yield loci for different materials and the associated achievable strain ratios ( $\delta\epsilon_{zz}/\delta\epsilon_{\theta\theta}$ ) with and without friction between the pellet and the sample.

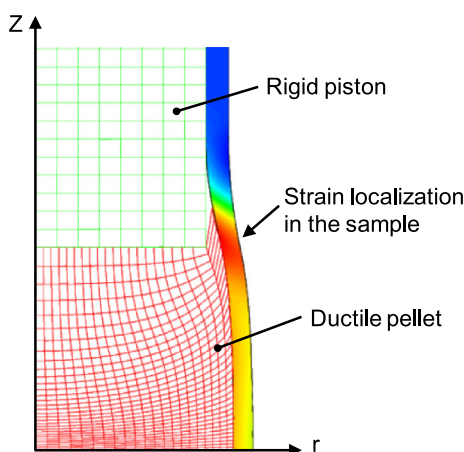


**FIGURE 14** Calculated equivalent strain field in the sample and the predicted zone of strain localization due to an excessive axial force.

effects between the ductile pellet and the sample will affect the achievable value. In addition, the preceding phenomenological explanation assumes that the material has perfectly plastic behaviour, but in reality, strain hardening can affect the achievable strain ratio. In this case, a detailed finite element analysis that accounts for effects such as friction and strain hardening can provide a more accurate analysis of the achievable strain ratio.

### 5.3 | Simulations of the limiting strain ratio

Finite element simulations with the CAST3M code predict that if the axial load is too great, then the axial force will be too large, and the sample will fail near the interface between the piston and the pellet. Figure 14 shows the predicted failure zone for such a case, using the model for Zircaloy-4 at 25°C<sup>[30]</sup> presented in Section 3.1.2. Failure can occur in this zone prior to any significant plastic deformation of the centre of the sample. It is also possible for failure to occur in this zone after a significant amount of plastic deformation has occurred, as shown in the figure.

It is possible to increase the attainable strain biaxiality by reinforcing the sample in the zone of strain localization. Alternatively, the sample could be reduced in thickness in the area of interest near the centre, as was done in a previous study,<sup>[8]</sup> in which the wall thickness was reduced by 9% over the central portion of its length. The tests on modified samples were able to reach greater strain biaxialities and were used to create a model for the ductile failure of Zircaloy-4 as a function of the biaxiality. It should be noted that great care must be taken to ensure that any modifications to the sample do not affect the experimental results.

## 5.4 | Modelling friction effects

As shown in Figure 8, the finite element simulations predict that the coefficient of friction between the ductile pellet and the sample has a significant effect on the strain ratio in the EDCT test. However, accurately simulating this frictional interaction is not trivial. In this study, Coulomb's law of friction was employed, assuming a constant value for the coefficient of friction. Of the three values of coefficient of friction used in the simulations (0.1, 0.2 and 0.4), 0.4 leads to the closest agreement with the experimental results. However, this result does not necessarily mean that Coulomb's law of friction with a coefficient of 0.4 is an accurate representation of the frictional interaction between the PTFE pellet and the sample. In reality, this frictional interaction is probably very complex and may not be accurately represented by a constant value. For example, researchers who have studied the sliding of PTFE against metal surfaces have found that the ratio of the friction force to the normal force often varies with contact pressure, sliding speed and surface conditions.<sup>[32,34]</sup> At the high contact pressures that occur between the pellet and the sample during an EDC test, an accurate representation of the friction effects would require a detailed model, which will be the subject of future work.

## 6 | CONCLUSIONS

This study examines some of the capabilities and limitations of EDCT tests, which are laboratory experiments that can be used to measure the failure strain of tubular samples as a function of the strain ratio ( $\epsilon_{zz}/\epsilon_{\theta\theta}$ ). The strain ratio can have a significant effect on the hoop strain at failure, as shown by the tests performed in this study on CWSR Zircaloy-4 tubes at 25°C. The two devices used in this study allow EDCT experiments to be performed on tubular samples, with different strain ratios using a standard tensile testing machine. The first device was introduced in a previous study and applies an axial force to the ends of the sample via plastically deforming tensile rods. By altering the geometry of the rods, the strain ratio in the centre of the sample can be modified. The axial force required is dependent on the sample's mechanical behaviour and must be determined before the test in order to design the tensile rods, for example, using finite element simulations. This method is a good means of producing different strain ratios for a given sample material, but it requires precise knowledge of the sample's mechanical behaviour. The second EDCT device was developed in the current study, and it applies a controlled axial displacement to the ends of the sample and allows EDCT tests to be performed without precise knowledge of the sample's mechanical behaviour. Using this device, tests were performed at a strain ratio of 0.1 on Zircaloy-4 tubes in cold-worked, CWSR and recrystallized states. For these three materials, the final strain ratios were similar (0.11, 0.09 and 0.07, respectively), but the hoop strains at failure were significantly different (7%, 12% and 21%, respectively). Thus, this EDCT method is a good means of reproducing a given strain ratio for samples with slightly different mechanical properties, for example, in order to study the effect of cold-work or a heat treatment on the failure strain.

EDCT tests can produce a wide range of strain ratios, but there is an upper limit on the strain ratio that can be obtained in the sample. For EDCT tests on CWSR Zircaloy-4 tubes at 25°C, the limiting strain ratio was approximately 0.4. The limiting strain ratio for a perfectly plastic material can be estimated from the shape of the yield locus of the sample material and the friction conditions between the components. For a material that strain hardens, the limiting value can be estimated using finite element simulations.

### ACKNOWLEDGEMENTS

The authors would like to thank the project *GAINES* of the French *Institut Tripartite CEA-EDF-Framatome* for supporting this study and Johann Pegaitaz for assisting with the experiments.

### DATA AVAILABILITY STATEMENT

Research data are not shared.

### ORCID

M. Bono  <https://orcid.org/0000-0002-2403-5553>

### REFERENCES

- [1] J. Desquines, D. A. Koss, A. T. Motta, B. Cazalis, M. Petit, *J. Nucl. Mater.* **2011**, *412*, 250. <https://doi.org/10.1016/j.jnucmat.2011.03.015>
- [2] W. F. Hosford, R. M. Caddell, *Metal Forming Mechanics and Metallurgy*, Prentice-Hall, Englewood Cliffs, New Jersey **1993**.

- [3] K. L. Murty, I. Charit, *Prog. Nucl. Energy* **2006**, *48*, 325. <https://doi.org/10.1016/j.pnucene.2005.09.011>
- [4] T. Shinozaki, Y. Udagawa, T. Mihara, T. Sugiyama, M. Amaya, *J. Nucl. Sci. Technol.* **2016**, *53*, 1426. <https://doi.org/10.1080/00223131.2015.1123658>
- [5] F. Li, T. Mihara, Y. Udagawa, M. Amaya, *J. Nucl. Sci. Technol.* **2019**, *56*, 432. <https://doi.org/10.1080/00223131.2019.1592723>
- [6] F. Yunchang, D. A. Koss, *Metall. Trans. A* **1985**, *16*, 675. <https://doi.org/10.1007/BF02814242>
- [7] M. Bono, Dispositif pour essai bi-axé à l'aide d'un unique vérin, Patent FR3041097, **2017**. <https://data.inpi.fr/brevets/FR3041097>
- [8] A. Zouari, M. Bono, D. Le Boulch, T. Le Jolu, J. Crépin, J. Besson, *J. Nucl. Mater.* **2021**, *554*, 153070. <https://doi.org/10.1016/j.jnucmat.2021.153070>
- [9] M. Bono, A. Zouari, Dispositif pour appliquer sur un échantillon une charge bi-axiale différentielle, Patent FR3101421, **2021**. <https://data.inpi.fr/brevets/FR3101421>
- [10] ASTM Designation: B 811-02. Standard specification for wrought zirconium alloy seamless tubes for nuclear reactor fuel cladding. Annexe A1. Room temperature closed-end burst testing procedure for zirconium alloy nuclear fuel cladding tubes.
- [11] B. H. Jones, *Exp. Mech.* **1968**, *8*, 10. <https://doi.org/10.1007/BF02326245>
- [12] M. A. Kaplan, G. A. Rowell, *J. Appl. Mech.* **1975**, *42*, 15. <https://doi.org/10.1115/1.3423509>
- [13] M. Bono, R. Limon, D. Le Boulch, *Int. J. Mech. Sci.* **2018**, *144*, 765. <https://doi.org/10.1016/j.ijmecsci.2018.06.026>
- [14] L. P. Mikkelsen, V. Tvergaard, *J. Mech. Phys. Solids* **1999**, *47*, 953. [https://doi.org/10.1016/S0022-5096\(98\)00062-3](https://doi.org/10.1016/S0022-5096(98)00062-3)
- [15] S. Boumaiza, J. P. Cordebois, M. Brunet, G. Nefussi, *Int. J. Mech. Sci.* **2006**, *48*, 674. <https://doi.org/10.1016/j.ijmecsci.2005.12.012>
- [16] M. N. Cinbiz, N. R. Brown, K. A. Terrani, R. R. Lowden, D. Erdman III, *Ann. Nucl. Energy* **2017**, *109*, 396. <https://doi.org/10.1016/j.anucene.2017.05.058>
- [17] M. N. Cinbiz, M. Gussev, K. Linton, K. A. Terrani, *Ann. Nucl. Energy* **2019**, *127*, 30. <https://doi.org/10.1016/j.anucene.2018.11.051>
- [18] M. N. Cinbiz, T. Koyanagi, G. Singh, Y. Katoh, K. A. Terrani, N. R. Brown, *J. Nucl. Mater.* **2019**, *514*, 66. <https://doi.org/10.1016/j.jnucmat.2018.11.023>
- [19] N. R. Brown, B. E. Garrison, R. R. Lowden, M. N. Cinbiz, K. D. Linton, *J. Nucl. Mater.* **2020**, *539*, 152352. <https://doi.org/10.1016/j.jnucmat.2020.152352>
- [20] T. M. Link, D. A. Koss, A. T. Motta, *Nucl. Eng. Des.* **1998**, *186*, 379. [https://doi.org/10.1016/S0029-5493\(98\)00284-2](https://doi.org/10.1016/S0029-5493(98)00284-2)
- [21] Y. Mishima, *J. Nucl. Sci. Technol.* **1966**, *3*, 294. <https://doi.org/10.1080/18811248.1966.9732327>
- [22] A. Garlick, *J. Nucl. Mater.* **1973**, *49*, 209. [https://doi.org/10.1016/0022-3115\(73\)90009-3](https://doi.org/10.1016/0022-3115(73)90009-3)
- [23] V. Grigoriev, R. Jakobsson, D. Schrire, R. Kesterson, D. Mitchell, H. Pettersson, Impact of corrosion on rapid deformation capabilities of Zirlo™ cladding, RIA Topical Meeting (OECD/CSNI), Cadarache, France, May 13–14, **2002**.
- [24] O. Dufourneaud, A.G. Varias, V. Grigoriev, R. Jakobsson, D. Schrire, Numerical simulation of the expansion-due-to-compression test, Fuel Safety Research Specialists' Meeting, At JAERI, Tokai, Japan **2002**.
- [25] P. Magnusson, A. M. Alvarez-Holston, K. Ammon, G. Ledergerber, M. Nilsson, D. Schrire, K. Nissen, J. Wright, *Nuclear Eng. Technol.* **2018**, *50*, 246. <https://doi.org/10.1016/j.net.2017.12.013>
- [26] J. C. Wood, B. A. Surette, I. M. London, J. Baird, *J. Nucl. Mater.* **1975**, *57*, 155. [https://doi.org/10.1016/0022-3115\(75\)90256-1](https://doi.org/10.1016/0022-3115(75)90256-1)
- [27] B. N. Nobrega, J. S. King, G. S. Was, S. B. Wisner, *J. Nucl. Mater.* **1985**, *131*, 99. [https://doi.org/10.1016/0022-3115\(85\)90448-9](https://doi.org/10.1016/0022-3115(85)90448-9)
- [28] A. Hellouin de Menibus, Q. Auzoux, P. Mongabure, V. Macdonald, T. Le Jolu, J. Besson, J. Crépin, *Mater. Sci. Eng. A* **2014**, *604*, 57. <https://doi.org/10.1016/j.msea.2014.02.075>
- [29] CEA, [www-cast3m.cea.fr](http://www-cast3m.cea.fr), **2015**. CEA developed and holds all rights to the CAST3M finite element code.
- [30] M. Le Saux, J. Besson, S. Carassou, C. Poussard, X. Averty, *J. Nucl. Mater.* **2008**, *378*, 60. <https://doi.org/10.1016/j.jnucmat.2008.04.017>
- [31] R. Hill, *The Mathematical Theory of Plasticity*, The Clarendon Press, Oxford **1950**.
- [32] S. K. Biswas, K. Vijayan, *J. Mater. Sci.* **1988**, *23*, 1877. <https://doi.org/10.1007/BF01115734>
- [33] S. K. Biswas, K. Vijayan, *Wear* **1992**, *158*, 193. [https://doi.org/10.1016/0043-1648\(92\)90039-B](https://doi.org/10.1016/0043-1648(92)90039-B)
- [34] H. Unal, A. Mimaroglu, *Ind. Lubric. Tribol.* **2003**, *55*, 178. <https://doi.org/10.1108/00368790310480362>
- [35] O. Dufourneaud, A.G. Varias, V. Grigoriev, R. Jakobsson, D. Schrire, Elastic-plastic deformation of a nuclear fuel cladding specimen under the internal pressure of a polymer pellet, WCCM V Fifth World Congress on Computational Mechanics, Vienna, Austria, July 7–12, **2002**.
- [36] M. Dostál, M. Valach, J. Zymák, Extension of parametric calculations of the expansion due to compression test using FEM model, 2011 Water Reactor Fuel Performance Meeting, Chengdu, China, Sept. 11–14, **2011**.
- [37] M. Le Saux, C. Poussard, X. Averty, C. Sainte Catherine, S. Carassou, J. Besson, High temperature expansion due to compression test for the determination of a cladding material failure criterion under RIA loading conditions, Proceedings of the 2007 International LWR Fuel Performance Meeting, San Francisco, California, September 30–October 3, **2007**.
- [38] S. Basak, S. K. Panda, *Int. J. Mech. Sci.* **2019**, *151*, 356. <https://doi.org/10.1016/j.ijmecsci.2018.10.065>
- [39] T. Jin, Z. Zhou, J. Qiu, Z. Wang, D. Zhao, X. Shu, S. Yan, *J. Alloys Compd.* **2018**, *738*, 79. <https://doi.org/10.1016/j.jallcom.2017.12.160>
- [40] M. O. Andar, T. Kuwabara, D. Steglich, *Mater. Sci. Eng. A* **2012**, *549*, 82. <https://doi.org/10.1016/j.msea.2012.04.009>
- [41] D. C. Drucker, *Proceedings First U.S. National Congress of Applied Mechanics* **1951**, 487.

**How to cite this article:** M. Bono, A. Zouari, T. Le Jolu, D. Le Boulch, H. Tabouret, J. Crépin, J. Besson, *Strain* **2023**, e12462. <https://doi.org/10.1111/str.12462>